REMOTE SENS. ENVIRON. 41:227–237 (1992)

SPOT Calibration at the La Crau Test Site (France)

R. Santer, X. F. Gu,† G. Guyot,† J. L. Deuzé,* C. Devaux,* E. Vermote,* and M. Verbrugghe†*

**Laboratorie d'Optique Atmosphérique, Université de Lille I, Villeneuve d'Ascq, France*
†INRA Bioclimatologie, Montfavet, France

In-flight calibrations of SPOT1 were performed in 1989 using a French site located in La Crau (southeastern France). A full description of the procedure is presented which includes both the characterization of the ground and of the atmosphere. To predict the radiance at the satellite level, we take into account the nonlambertian properties of the test site and the surrounding contribution. A detailed error budget is carefully conducted; the overall error of the method is around ± 3%. The three calibrations performed are self-consistent and are in close agreement with calibration data obtained by CNES for XS2 and XS3. A discrepancy of 8% is observed for XS1 and its origin is under study.

INTRODUCTION

In France, the National Center for Space Studies (CNES) is highly concerned with the calibration of HRV instruments aboard SPOT. From the preflight calibration (Begni, 1985), two internal calibration devices (Dinguirard and Maisoneuve, 1980), using respectively the Sun and a lamp as light sources, can be used to follow the sensitivity loss of the system. Moreover, an in-flight calibration has been conducted by Slater's team throughout the lifetime of SPOT1 using the method developed for Landsat TM calibration (Slater et al., 1987). This method combines the measurement of the reflectance of a test site (White Sands in New Mexico or Edward Base in California) with the characterization of the atmosphere at the time of the satellite overpass. Using an atmospheric transfer code, the incoming radiance at the sensor is predicted and compared to digital counts registered over the test site.

For the preparation of SPOT 4 and 5 missions, CNES wished to develop an alternative calibration site in Europe. The choice of the site was the object of a previous investigation divided into two successive steps. From a first study performed on satellite data, several potential sites over Europe and Northern Africa were compared (Rouquet, 1987) and the site at La Crau was selected. Ground-based and airborne reflectance measurements of La Crau enabled us to define the position of the test site and to characteize its bidirectional properties and its spatial and temporal variabilities (Gu et al., 1990).

The aim of this article is to present the results of the last step of the analysis and the results of two SPOT calibration campaigns conducted in 1989 in order to validate the methodologies used.

Address correspondence to Dr. Xing-Fa Gu, INRA Bioclimatologie, BP 91, 84143 Montfavet Cedex, France.
Received 1 March 1992.

0034-4257/92/$5.00

655 Avenue of the Americas, New York, NY 10010

GROUND REFLECTANCE MEASUREMENTS

The calibration site, a 400 × 400 m^2 area, is located in the center of "La Crau Seche," a 60 km^2 flat pebbly area in southeastern France (longitude: 4.87°E, latitude: 43.50°N), on the eastern bank of the Rhone river and about 50 km northwest of Marseille (Gu et al., 1990). This area has a dry and sunny Mediterranean climate. The soil is mainly composed of pebbles and is sparsely covered by a low vegetation. Its optical properties vary little within the year.

A detailed description of the measurement procedure is reported by Gu et al. (1992). SPOT simulation radiometers (Guyot et al., 1984) simultaneously measure the reflected directional radiance and the incident hemispherical irradiance in the SPOT channels. The ground bidirectional reflectance is obtained by ratioing the two measurements and a calibration is done, using a halon panel. Departures of the irradiance head and of the reflectance panel from the cosine law have been measured and the corresponding corrections are introduced in the data reduction (Gu, 1991). The analysis of the sampling variance of the 400 m × 400 m test site enabled us to define the number of measurements necessary for obtaining a given accuracy (Dagnelie, 1970). With 100 samples (0.6 m in diameter) the error on the ground reflectance is lower than ±2% for SPOT Channels 1 (XS1) and 2 (XS2) and lower than ±1% for Channel 3 (XS3) (Gu et al., 1990). For the direct-direct path, nadir reflectance measurements were performed at the time of satellite overpass (within ±30 min). For SPOT off-nadir viewing a correction was applied using a set of bidirectional measurements (Guyot et al., 1989). As these measurements are performed with a mobile boom and are time-consuming, they were restricted to a few samples. In order to reduce the error due to the view angle correction, the future ground-level reflectance measurements will be performed using a new support enabling measurement of the ground radiance with the same geometry as SPOT (Gu et al., 1992).

Two measurement campaigns were performed in March and June 1989. All the available SPOT windows were recorded, and only three dates were used considering the atmospheric conditions: 22 March, 7 and 13 June. For these experimental calibration campaigns, only multispectral images were acquired with the HRV2 instrument.

Table 1 gives the geometrical conditions of the observations. Table 2 reports, for each date, the number of samples, the mean value of the reflectance measured in the SPOT channels, and their standard deviations. It must be pointed out that the number of measurements is limited and the accuracy of the reflectance estimate is reduced as compared to an ideal figure of 400 samples allowing an accuracy better than ±1% (Gu et al., 1990). For these measurements only one radiometer was available and 100 measurements required about 1 h. Moreover, on 7 June, cloudy conditions occuring before the SPOT overpass reduced this number.

ATMOSPHERIC MEASUREMENTS

In order to apply the atmospheric corrections, it is necessary to characterize the aerosols and also the amount of gases which absorb and scatter the light in the SPOT bands. The characteristics of the aerosols (size distribution function, spectral optical thickness) and the atmospheric gas transmission are determined from passive optical measurements at ground level and radiosonde data. The Rayleigh scattering due to gas molecules, which depends on atmospheric pressure and wavelength, is deduced from barometric measurements at ground level.

Table 1. Geometric Conditions of the SPOT Observations[a]

Date	*Time of Overpass (U.T.)*	θ_s (°)	ϕ_s (°)	θ_v (°)	ϕ_v (°)
22-03	10.42	45.9	156.6	2.7	99
07-06	11.01	22.4	156.4	25.5	279
13-06	10.46	33.8	155.8	3.7	99

[a] θ = zenith angle; ϕ = azimuth angle; s = sun angle; v = view angle.

Table 2. Mean Reflectances (ρ) of la Crau in the Three SPOT-HRV Bands and Their Standard Deviations (σ)[a]

Date	*Parameters*	*XS1*	*XS2*	*XS3*
22-03	ρ	12.3	17.7	29.8
(106)	σ	1.3	1.8	1.6
07-06	ρ	14.2	19.8	27.7
(56)	σ	1.1	1.4	1.4
13-06	ρ	16.0	22.2	30.0
(108)	σ	1.1	1.3	1.1

[a] The number of measurements is indicated in parentheses under the date.

Description of the Measurements

Different radiometers measure the extinction of the solar beam in the range 0.45–2.2 μm. A single wavelength radiometer (at 450 nm) (ETAL) was calibrated on the extraterrestrial irradiance during stratospheric flights at an altitude higher than 25 km. The other radiometers are cross-calibrated directly in the blue band. For the other channels, the calibration is initialized using the classical Langley–Bouguer plotting with a linear regression on the logarithm of the radiometer output voltage $V(\lambda)$ and the air mass M:

$$\log\ V(\lambda) = \log\ V_s(\lambda) - \delta(\lambda)M. \qquad (1)$$

Equation (1) provides the intercept $V_s(\lambda)$ and the slope $\delta(\lambda)$ corresponding to the total atmospheric optical thickness. It is well known that the stability of the atmosphere, required for this method, is a first approximation. The suggested improvement consists in monitoring the variation of the optical thickness as a function of the time t (from the Langley plot) with the assumption that it is mainly due to variations of the aerosol optical thickness, $\delta_a(t)$. We then obtain

$$\frac{\Delta\delta_a(t,\lambda)}{\delta_a(\lambda)} = \frac{\Delta\delta_a(t,450\ \text{nm})}{\delta_a(450\ \text{nm})}. \qquad (2)$$

Assuming that the aerosols are stable in nature, the mean value of δ_a at λ and 450 nm is derived from the Langley linear regression after removing the Rayleigh contribution. The instantaneous variations of the aerosol optical thickness at 450 nm are measured by the calibrated radiometer ETAL. Plotting of $\log\ V(\lambda) + \Delta\delta_a(t,\lambda)\cdot M$ gives a better estimate of $V_s(\lambda)$ and $\delta_a(\lambda)$.

Aureole measurments are also performed at $\lambda = 850$ nm. The radiometer with 1° field of view initially aims at the Sun. Then a small rotation in azimuth allows collection of measurements in the range of the scattering angle, between 2° and 30°. The diffuse radiance is proportional to the atmosphere phase function from which a first estimate of the aerosol phase function can be deduced. This first estimate is then used to correct for the effect of multiple scattering, using a simple iterative method proposed by Weinman et al. (1975).

The last measurements consist of scans in the principal plane of the radiance and of the polarization ratio. The photopolarimeter described by Herman et al. (1986) has two bands at 850 nm and 1650 nm in order to minimize the Rayleigh scattering contribution.

Aerosol Characterization

To apply the atmospheric corrections, the aerosols must be characterized with three parameters: their optical thickness $\delta_a(\lambda)$, their size distribution $n(r)$, and their refractive index $(m - ik)$. The aerosol thickness is the fundamental parameter directly produced by the extinction measurements. The main problem consists in the determination of the last two parameters.

We are not concerned with the actual complexity of the aerosols, by either their composition and or their vertical distribution. We just need a convenient description of the medium which allows us to retrieve the optical properties in order to apply the atmospheric corrections. The aerosol model used corresponds to a "modified" Junge size distribution with

$$\begin{aligned} n(r) &= Cr_0^{\nu} \quad \text{if } r \leqslant r_0, \\ n(r) &= Cr^{\nu} \quad \text{if } r > r_0, \end{aligned} \qquad (3)$$

and a particle refractive index $(m - ik)$ independent of the size.

It is then necessary to define our strategy concerning the inversion. As demonstrated by Santer (1984), the inversion of the polarization and of the radiance at two wavelengths permits retrieval of the main optical properties of the medium. The inversion is conducted as follows: First we use a simple but accurate approximate of the signal (Deuzé et al., 1987), which includes the Rayleigh scattering, the multiple scattering, and a boundary condition, corresponding to a lambertian reflector. Then, for a given refractive index m and a set of r_0 values, we adjust the polarization ratio at 1650 nm. Finally the 850 nm retrieval provides a unique solution (r_0,ν).

As an example, we give the restitution of polarization measurements (Fig. 1) and the radiance (Fig. 2) performed on 7 June, around 6:00 a.m., when the sun was low. The restitution of the polarization can be achieved regardless of the particle refractive index. To retrieve the polarization ratio around $\theta = 100°$, it is necessary to introduce larger particle size when the refractive index decreases. Conversely, the aureole measurements are not sensitive to the refractive index (major contribution of the diffraction) but highly dependent upon the particle size. The comple-

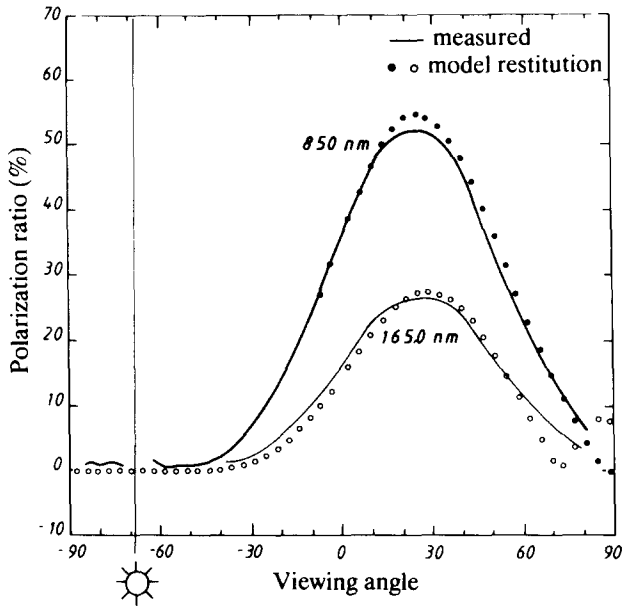

Figure 1. Measured polarization ratio compared to the restitution with an aerosol model defined by $r_0 = 0.15$ μm, $\nu = -3.7$, $m = 1.50$, and $\delta_a^{850} = 0.056$. The measurements were performed with a low sun at 6:00 a.m. on 7 June 1989.

mentarity between polarization and aureole measurements is illustrated in Figure 3, where a typical value of $m = 1.50$, characteristic of continental materials, appears to be suitable.

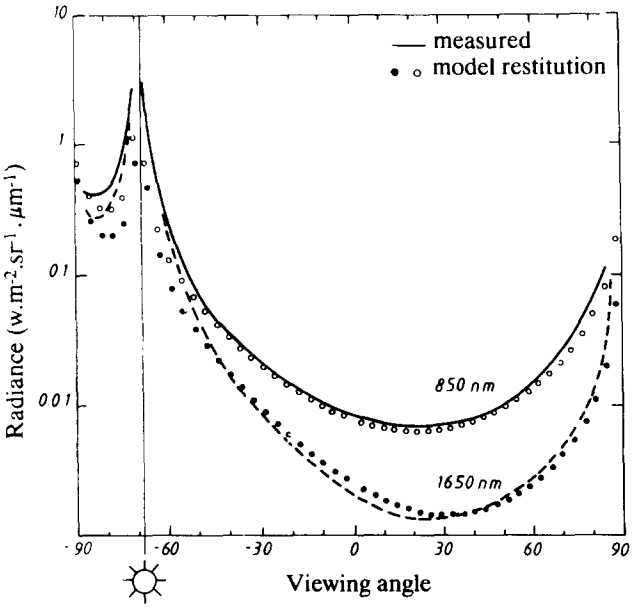

Figure 2. Measured radiance compared to the restitution with an aerosol model defined by $r_0 = 0.15$ μm, $\nu = -3.7$, $m = 1.50$, and $\delta_a^{850} = 0.056$. The measurements were performed with a low sun at 6:00 a.m. on 7 June 1989.

Gaseous Contents

At a given place, the ozone amount can be determined with an acceptable accuracy, from the seasonal values given by London et al. (1976). For the water vapor content, two weather stations bound the site: Marignane (10 km SE of the site) and Nimes (40 km NW). From the two stations we obtain temperature and relative humidity (under screen) from which we derive, by linear interpolation, the water vapor density at ground level on the test site. We have also radiosoundings at midnight and noon performed at Nimes. The integrated water vapor content on the site, at the time of the SPOT overpass, is the result of linear spatiotemporal interpolations between the ground level measurements and the radiosondages.

In fact, the ground-based station can control this information. The extinction measurements, including the Chapuis band and the aerosol model, is sufficiently defined to predict, from outside measurements, their contribution in this band (Biggar et al., 1990). In the same way, a differential technique (Frouin and Gautier, 1987) associates a broad and a narrow band filter in the water vapor band at 950 nm to derive the integrated amount (Table 3).

Results

Table 4 gives, for three days of measurements, the aerosol optical thickness as measured in the SPOT bands; the two flexible parameters (r_0,ν) of the Junge size distribution are derived from the polarization measurements, and the refractive index is the result of the aureole retrieval for 22 March and 7 June. For 13 June, the characterization of the aerosols was done only by extinction measurements with a portable sun-radiometer working between 0.45 μm and 0.85 μm. The slope of the Junge size distribution follows the spectral dependence of $\delta_a(\lambda)$ while the refractive index value determined on 7 June is used.

We have to point out that the aerosol model is close to the standard continental model (Deirmendjian, 1964) defined by $r_0 = 0.1$ μm, $\nu = -4$, $m = 1.50$. The extremely good visibilities observed on 22 March and 7 June correspond to a Mistral regime, the continental dry wind which blows in the Rhone valley.

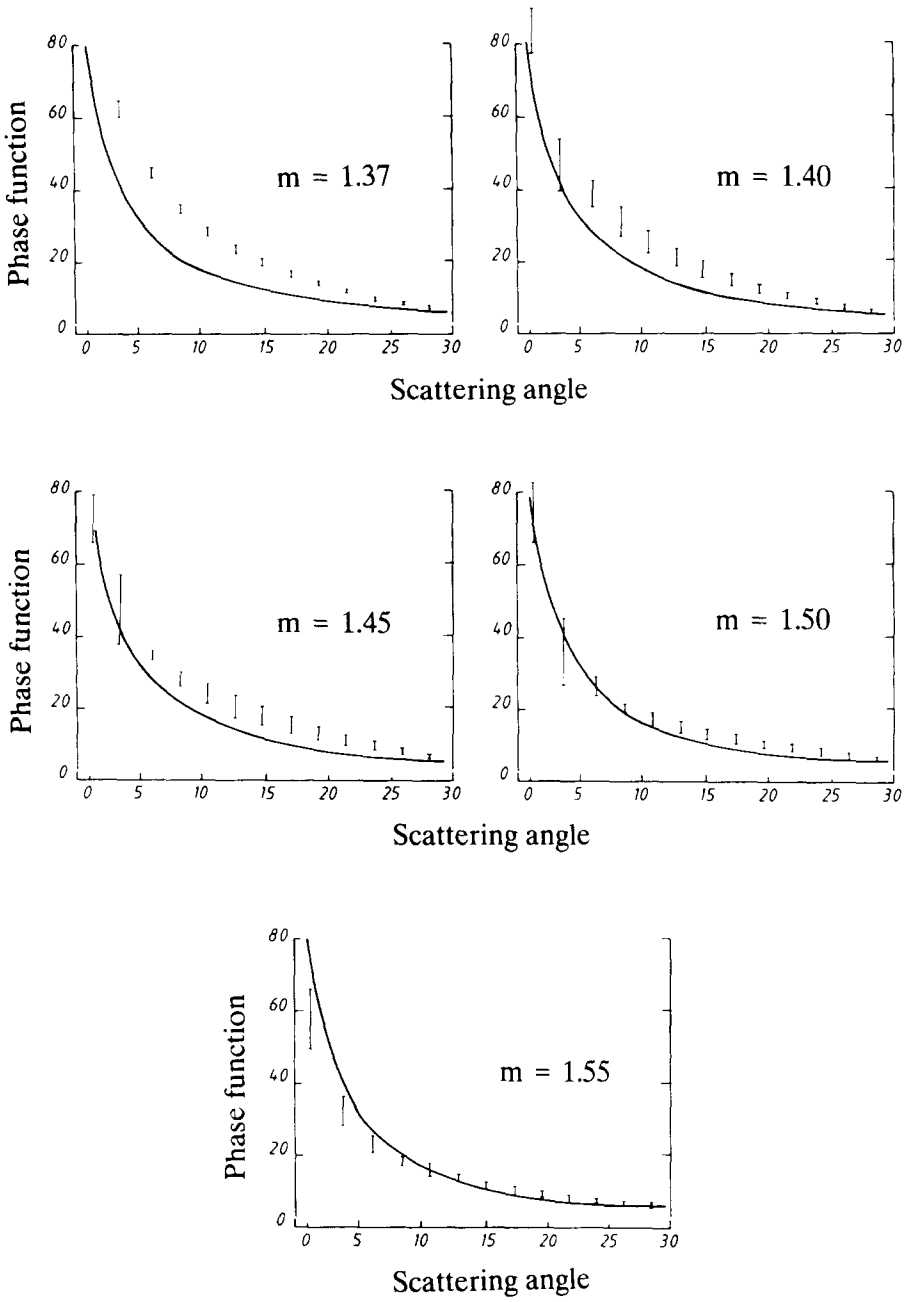

Figure 3. Restitution of the aureole for the measurements on 7 June. Aureole measurements are converted into phase function (continuous line) and compared to phase function computed for models deduced from the inversion of the polarization at different refractive indices. Error bars result from inaccuracies introduced in the measurements. The computations are normalized at $\theta = 30°$ and the increase of the error bars in the forward scattering is a direct consequence.

COMPUTATION OF THE SIGNAL

Standard Computation

To express the apparent reflectance ρ^*_i in Channel i, we uncouple absorption and scattering with

$$\rho^*_i = T^i_g \rho^0_i. \tag{4}$$

The gaseous transmittance T^i_g is computed using the "5S" code (Tanré et al., 1990). The spectral response of the SPOT internal filters R^i_λ are provided by CNES and the other inputs for ozone and water vapor are the integrated values. The reflectance ρ^0_i corresponds to the reflectance observed over a lambertian reflector ρ_g for a nonab-

Table 3. Atmospheric Water Content and Ozone Concentration for the Three Days of Measurements

Date	U_{H_2O} *(g cm^{-2})*	U_{O_3} *(cm atm)*
22-03	1.83	0.390
07-06	1.27	0.383
13-06	1.27	0.388

Table 4. Aerosol Characteristics

Date	Optical Thickness			Size Distribution		Refraction Index
	XS1	XS2	XS3	r_0	ν	(m)
22-03	0.049	0.042	0.032	0.10	−4.0	1.50
07-06	0.072	0.065	0.056	0.15	−3.7	1.50
13-06	0.334	0.285	0.218	0.10	−4.0	1.50

sorbing atmosphere. The computation is achieved using the method of successive orders of scattering (Deuzé et al., 1989). The inputs are the inverted aerosol model (r_0, ν, m, δ_a^i), mixed with the Rayleigh scattering, assuming a scale length of 2 km for the aerosols and the ground reflectance ρ_g.

The computation is monochromatic and the Rayleigh and aerosol optical thickness δ have been integrated over the filter response:

$$\delta = \frac{\int_0^\infty E_s(\lambda) R_\lambda^i \delta(\lambda)\ d\lambda}{\int_0^\infty E_s^\lambda R_\lambda^i\ d\lambda}, \quad (5)$$

with

R_λ^i = spectral responsivity of the sensor,
E_s^λ = equivalent solar irradiance.

The spectral dependence of δ is in λ^{-4} for the Rayleigh and in $\lambda^{-\alpha}$ for the aerosols where the Angström coefficient α is derived from the measurements.

This basic version of the solution of the radiative transfer equation in a plane-parallel atmosphere does not take into account the actual nonlambertian properties of the surface and the spectral inhomogeneity of the target.

Departures from the Lambertian Approximation

The bidirectional properties of La Crau have been measured by Gu et al. (1991). For example, during summer, at the SPOT overpass time, the bidirectional reflectance decreases by about 10% in the specular direction and increases by 20% in the hot spot, compared to nadir measurements. The successive order transfer code is based on a Fourier series decomposition of the signal, and a suitable expansion of the boundary condition is

$$\rho(\mu_v,\mu_s,\phi_v-\phi_s) = \sum_{s=0}^{4} \rho^s(\mu_v,\mu_s)\ \cos(\phi_v-\phi_s), \quad (6)$$

with $\mu = \cos\theta$.

Since the surface reflection is quite isotropic, the Fourier series expansion is restricted to five terms. The components $\rho^s(\mu_v,\mu_s)$ are computed in a polynomial form for a complete set of bidirectional measurements at different solar elevations. The principle of reciprocity is used to double the available points. Figure 4 reports the relative error on ρ_i^0 if we neglect the bidirectionality of the reflectance. These computations, versus the view angle v_v, are done for three solar zenith angles, 30°, 50°, and 60°, for $\phi_v - \phi_s = 50°$, which closely corresponds to the SPOT azimuth angle (see Table 1).

The errors depend slightly upon the viewing angles and decrease with the increasing wavelength and with the decreasing atmospheric effects. Since they can be as high as 3%, the bidirectional effects have to be included in the calibration process. Fortunately the properties of the ground are quite stable with time, mainly in their angular distribution. We can then add extensive data collected prior to those collected the day of a SPOT calibration.

Effect of the Environment

If La Crau is reduced in size (about 10 km in diameter), the contribution of the surroundings

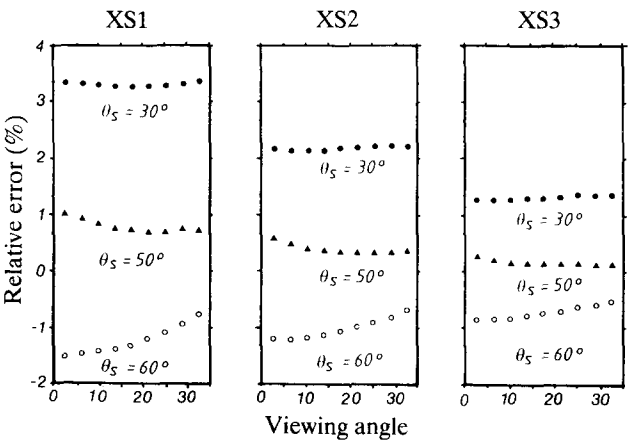

Figure 4. Relative difference between a lambertian target and la Crau in the vertical plan, perpendicular to the sun azimuth. The continental aerosol model is used with a visibility of 50 km. The simulations correspond to three sun zenith angles for each SPOT bands.

may then be significant. A simple case is proposed for computation in 5S: homogeneous disk surrounded by homogeneous ground. An immediate modification can be done by dividing the surroundings into elementary coronets. Figure 5 gives the average digital counts for coronets 200 m thick as measured by SPOT in the three bands. As reported in the Appendix, from the contrast of the digital counts between the target and its environment, and for a given atmosphere, we can derive the environmental effect. For example, for a visibility of 50 km with continental aerosols and a solar zenith angle of 30°, the environment, as shown in Figure 5, decreases the reflectance by 2% in XS1, 1.7% in XS2, and 0.4% in XS3, compared to a spatially uniform ground. Again it appears necessary to include this effect in a calibration procedure.

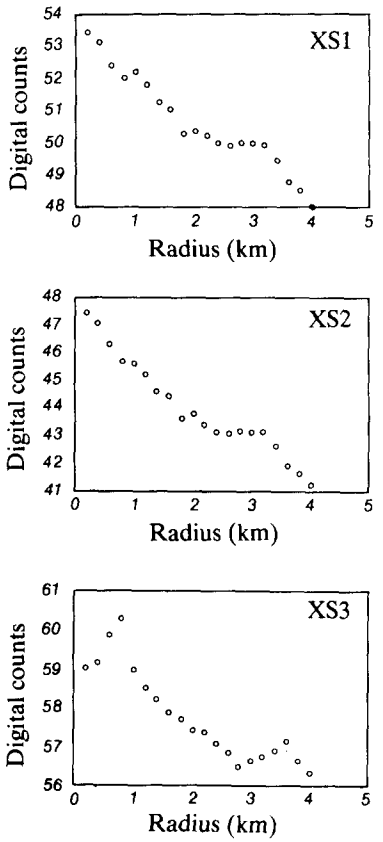

Figure 5. Variation of the mean digital counts of the SPOT image, as a fuction of the diameter of the circle centred on the test site, for the three SPOT channels.

CALIBRATION AND RELATED ERRORS

Calibration Coefficients

The incoming parameter at the sensor is the integrated radiance

$$L_i = \oint_0^\infty R_i^\lambda L_\lambda \, d\lambda \quad (\text{w m}^{-2} \text{ sr}^{-1} \ \mu\text{m}^{-1}) \quad (7)$$

with L_λ = monochromatic radiance at the sensor.

Generally, in order to be independent of the absolute amplitude of the spectral response, the integrated radiance L_i is transformed into an equivalent radiance L_i^e:

$$L_i^e = \frac{L_i}{\oint_0^\infty R_\lambda^i \, d\lambda}. \quad (8)$$

Since the detection is linear, the calibration equation is

$$\text{DC}_i = A_i' L_i^e, \quad (9)$$

DC_i being the digital count and A_i' the calibration coefficient (counts per w m^{-2} sr^{-1} μm^{-1}). However, the viewing gain of SPOT HRV m_i can have eight integer values, $1 \leqslant m_i \leqslant 8$, associated with the signal amplifier. For this reason an absolute calibration coefficient A_i is defined and will be used in this study:

$$\text{DC}_i = A_i \ 1.3^{(mi-3)} L_i^e. \quad (10)$$

The digital count corrresponds here to the average value for the 20 × 20 pixels of the test site reported in Table 5. The transfer code produces the apparent reflectance ρ^*_i related to L_i^e by

$$L_i^e = \mu_s E_{si}^i \rho^*_i / (\pi d^2), \quad (11)$$

where E_s^i is the equivalent solar irradiance (1845,

Table 5. Digital Counts Observed for the Three SPOT Bands

Date	*Parameters*	*XS1*	*XS2*	*XS3*
22-03	Mean	67.7	66.6	61.9
	Minimum	59	58	58
	Maximum	73	72	65
	Standard deviation	2.1	2.1	1.1
07-06	Mean	88.8	95.2	75.9
	Minimum	82	88	73
	Maximum	94	99	78
	Standard deviation	1.9	2.0	1.0
13-06	Mean	93.1	100.5	77.4
	Minimum	88	94	75
	Maximum	97	105	80
	Standard deviation	1.6	1.9	0.9

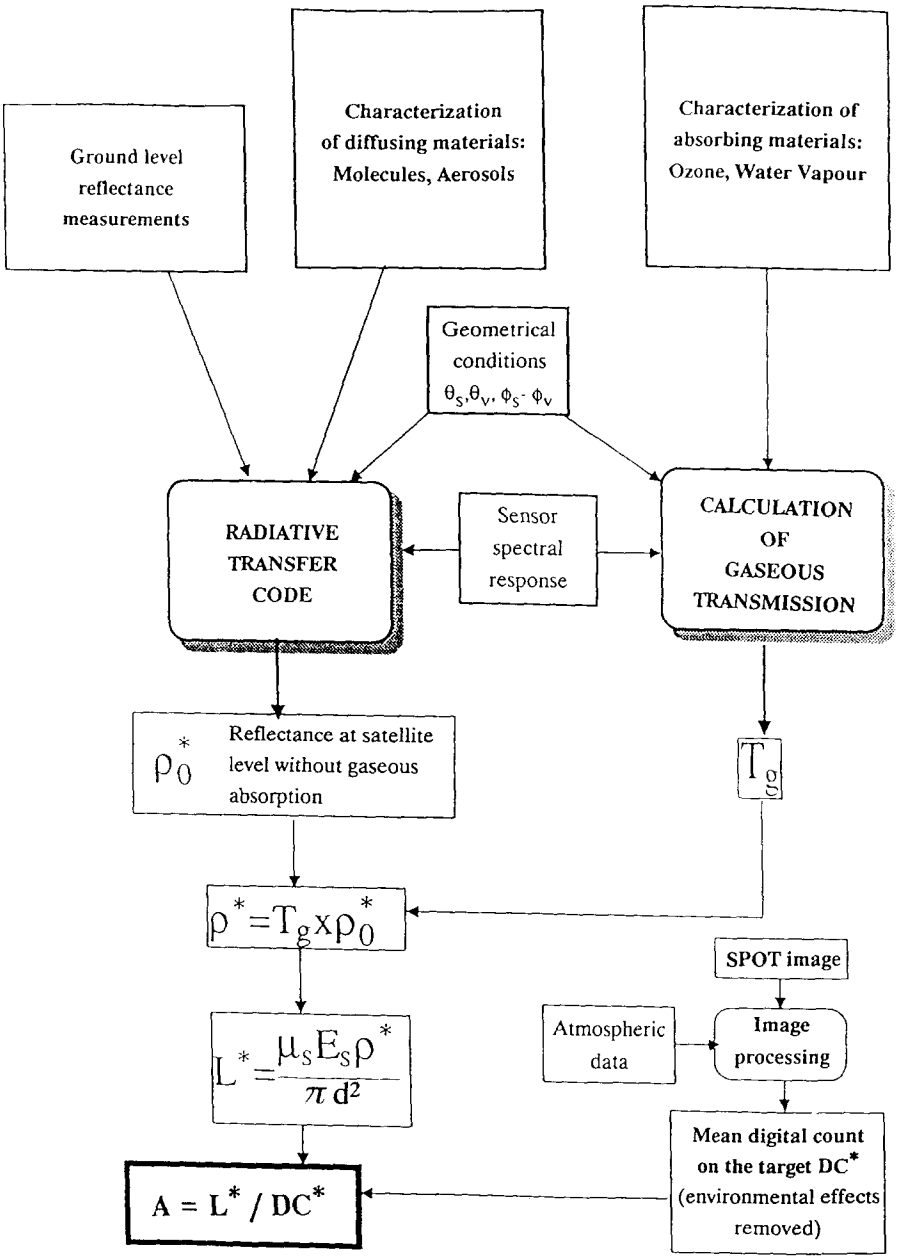

Figure 6. Flow chart representing the calibration procedure.

1575, and 1040 W m^{-2} μm^{-1} for SPOT1-HRV2 channels XS1, XS2, and XS3, respectively) and d the Earth–Sun distance (expressed in u.a.).

The flow chart reported in Figure 6 illustrates the complete calibration procedure. Ignoring the gaseous transmission, the apparent reflectance is computed with the optical parameters as first inputs. The boundary conditions correspond, for the direct to direct path, to the average measured values of the reflectances on the calibration site and, for the other terms, to an up-dated experimental description of the bidirectional function expended in a Fourier series. The gaseous transmission is computed separately using the "5S" code to balance the former result. The apparent reflectance is transformed into radiance. On the other hand, since the evolution of the environmental effect is achieved on the digital counts, we deconvolute the average value of the test site instead of correcting this surrounding effect on the predicted value of the outgoing radiance.

For the three dates, the calibration coeffi-

cients are reported in Table 6. We also reported the coefficients proposed by CNES (Dinguirard and Briottet, 1989) and also the relative difference between the two sets. For XS2 and XS3, the agreement is quite good and obviously within the error domains. The large discrepancies in XS1 are under investigation. One explanation lies in a possible yellowing of the lamp used for SPOT internal calibration. On the other hand, the calibration method applied to SPOT1 HRV1 and Landsat5 TM give consistent results compared with the calibration performed by Slater's team with a difference ranging between 0% and 6% (Gu, 1991).

Error Budget

Table 7 gives a detailed error budget for 7 June. The uncertainties on R_λ^i correspond to CNES specifications. The impacts of R_λ^i inaccuracies are on the determination of E_s^i and on the computation of the signal (mainly on gaseous transmission). The instrumental noises are proportional to μ_s. The errors on the reflectance of the ground are computed according to Gu et al. (1991), taking into account the spectral response of the radiometer and the actual number of samples. The apparent contribution of the surface is weighted by the atmospheric transmittances, which reduce, in the same way, the error in the estimation of ground contribution. As expected, errors concerning the gaseous content are more significant in XS1 for O_3 and XS3 for H_2O. Uncertainties of the barometric pressure (δh_p) have been introduced for the Rayleigh scattering. For the aerosols, the error budget is more complex, resulting from errors in measurements of the optical thickness, the polarization ratio, and the aureole. Moreover, since our inversion scheme is not sensitive to the imaginary part of the refractive index, we introduced this parameter as arbitrarily defined as 5×10^{-3}. The transformation of the reflectance into radiance is affected by uncertainties in θ_s and E_s^i with its natural variation (within 0.2%), plus a systematic bias of 1%, depending on the data source. At last, we saw how to correct for the environmental effects and a residual inaccuracy appears.

Finally, Table 8 gives the errors as a quadratic sum. The errors are of the order of 3% except on 13 June because the visibility was low. Moreover, the atmospheric measurements were reduced to visible extinction measurements, and the error budget was adapted consequently.

Table 7. Detailed Error Budget on 7 June

Origin	Relative Error (%)		
	XS1	XS2	XS3
Spectral response	0.60	0.90	0.60
Instrumental noise	1.60	1.45	1.05
Apparent refl. of the target	1.95	1.97	1.60
Water vapor	0.30	0.31	0.52
Ozone	0.58	0.47	0.00
Molecules	0.12	0.05	0.01
Aerosols	0.61	0.48	0.36
E_s variation	0.20	0.20	0.20
E_s determination	1.00	1.00	1.00
Sun zenith angle	0.14	0.14	0.14
Surrounding effect	0.50	0.50	0.10

Table 6. Comparison of SPOT1-HRV2 Calibration Coefficients Determined from La Crau and from the Internal Calibration (CNES)

Date	Origin	XS1	XS2	XS3
22-03	Crau	0.518	0.376	0.555
	CNES	0.469	0.381	0.567
	Difference (%)	+10.4	−1.3	−2.3
07-06	Crau	0.505	0.391	0.562
	CNES	0.466	0.380	0.567
	Difference (%)	+8.4	+2.9	−0.9
13-06	Crau	0.495	0.389	0.561
	CNES	0.466	0.380	0.567
	Difference (%)	+6.2	+2.4	−1.1

CONCLUSIONS

The utility of La Crau as a calibration site for SPOT has been demonstrated. This site should be used on a routine basis at a biannual rate. For further campaigns some improvements are planned. The number of samples of the target reflectance will be increased by using a second radiometer. Moreover, the radiometers will be

Table 8. Relative Error (%) on Calibration Coefficients

Date	XS1	XS2	XS3
22-03	3.2	3.1	2.0
07-06	3.0	3.0	2.4
13-06	6.3	4.4	5.0

tilted in the SPOT viewing direction and measurements will be performed in the same azimuthal plane. For atmospheric measurements, global and diffuse measurements are planned in order to control the absorption of the aerosols.

The 1991 campaign at La Crau has been integrated in the European NASA ER2 campaign with special attention paid to intercalibration with AVIRIS, the JPL spectroimager, and with POLDER, a photopolarimetric camera developed at Lille. For more general purposes, the Appendix provides a suitable tool for introducing the surrounding effect from the image content.

APPENDIX

As proposed by Tanré et al. (1990), the upward reflectance is the sum of three different contributors:

1. The atmospheric path radiance ρ_a.
2. The contribution of the pixel of reflectance ρ:

$$T(\mu_s)\rho e^{-\delta/\mu v} \tag{12}$$

where $T(\mu_s)$ is the total transmittance (i.e., the downward global irradiance divided by the solar incident flux) and where $e^{-\delta/\mu v}$ describes the attenuation on the direct atmospheric path.

3. The surrounding effect which can be expressed as

$$T(\mu_s)\,\langle\rho\rangle\,t_d(\mu_v), \tag{13}$$

where T_d is the diffuse transmittance and where $\langle\rho\rangle$ is the mean reflectance of the environment, expressed as

$$\langle\rho\rangle = \int_0^\infty \rho(r)f(r)\ dr. \tag{14}$$

The environment function $f(r)$ describes the probability for a photon reflected by the ground at a distance r from the target center to be scattered within the solid angle Ω.

Finally, the sum of the contributions gives

$$\rho^0 = \rho_a + \frac{T(\mu_s)[\rho e^{-\delta/\mu v} + \langle\rho\rangle t_d(\mu_v)]}{1 - \langle\rho\rangle s} \tag{15}$$

where the multiple interactions between the ground and the atmosphere, introduced in the denominator, involved the spherical albedo s. We have to point out that Eq. (14) corresponds to a nadir observation. According to Tanré et al. (1990), this formulation is still valid up to a viewing angle of 30°, which is suitable for SPOT observations. The atmospheric functions ρ_a, T, t_d, and s are computed using the successive orders of scattering method for the relevant inputs.

The *in situ* measurements are restricted to the calibration site. The computation of the environmental effect is then based on the contrast

$$C(r) = \mathrm{DC}(r) / \mathrm{DC}(o) \tag{16}$$

between the digital counts observed at a distance r from the target and for the target. From Eqs. (14)–(16), it can be demonstrated that (Vermote, 1990)

$$\langle\rho\rangle = \frac{\rho_a(P-1) + P\rho T(\mu_s)e^{-\delta/\mu v}}{s\rho_a(P-1) + T(\mu_s)[T(\mu_v) - Pt_d(\mu_v)]}, \tag{17}$$

where

$$P = \int_0^\infty f(r)C(r)\ dr. \tag{18}$$

This study was supported by the Centre National d'Etudes Spatiales (CNES) under Contract n° 833/89/5935/00. We thank M. Herman (LOA) and M. Leroy (CNES) for helpful discussions.

REFERENCES

Begni, G. (1985), The radiometric calibration of the SPOT HRV sensors, in *Acta Polytechnica Scandinavia* (T. Friberg and Pirkko Oittinen, eds.), Proc. Image Science, Vol. 2, pp. 10–11.

Biggar, S. F., Santer, R. P., and Slater P. N. (1990), Irradiance-based calibration of imaging sensors, in *Proc. IGARSS '90*, Washington DC, May 1990, pp. 507–510.

Dagnelie, P. (1970), *Théorie et Méthodes Statistiques*, (J. Duclot S.A., ed.), Les Presses Agronomiques de Gembloux, A.S.B.S.L., Gembloux, Belgium, Vol. 2, 451 pp.

Deirmendjian, D. (1964), Scattering and polarization properties of water clouds and hazes in the visible and infrared, *Appl. Opt.* 3:187–196.

Deuzé, J. L., Herman, M. and Santer, R. (1987), Modélisation de l'état de polarisation du rayonnement atmosphérique ascendant. Partie 1 Atmosphère limitée par un sol lambertien, Rapport Contrat CNES.

Deuzé, J. L., Herman, M., and Santer, R. (1989), Fourier series expansion of the transfer equation in the atmosphere-ocean system, *J. Quant. Spectrosc. Transfer* 41:483–494.

Dinguirard, M., and Briottet, X. (1989), Bilan d'étalonnage absolu SPOT1. Troisième bilan semestriel, Rapport CNES S-NT-OB1-561-CN.

Dinguirard, M., and Maisoneuve, J. M. (1980), Description du dispositif d'étalonnage absolu de la caméra HRV, Rapport CNES Toulouse (France) S-NT-OB1-0090-CN.

Frouin, R., and Gautier, C. (1987), Calibration and NOAA-7 AVHRR, GOES-5, and GOES-6 VISSR / VAS solar channels, *Remote Sens. Environ.* 22:73–101.

Gu, X. F. (1991), Etalonnage et intercomparaison des données satellitaires en utilisant le site test de la Crau, Thèse doctorat, Université Paris VII, 260 pp.

Gu, X. F., Guyot, G., and Verbrugghe, M. (1990), Analyse de la variabilité spatiale d'un site test -Exemple de la Crau (France), *Photo-Interprétation* 90-1(5):39–52.

Gu, X. F., Guyot, G., and Verbrugghe, M. (1992), Evaluation of measurement errors in ground surface reflectance for satellite calibration, *Int. J. Remote Sens.*, forthcoming.

Guyot, G., Hanocq, J. F., Buis, J. P., and Saint, G. (1984), Mise au point d'un radiomètre de simulation de SPOT, *Second International Colloquium on Spectral Signatures of Objects in Remote Sensing*, Bordeaux, France, 12–16 September 1983, Ed. INRA Publ., Les Colloques de l'INRA n° 23, pp. 233–242.

Guyot, G., Gu, X. F., and Verbrugghe, M. (1989), Caractérisation des propriétés optiques du site de la Crau, Rapport Final Contrat 833 / CNES / 87 / 4891 / 00, INRA Bioclimatologie, Montfavet, France, 79 pp.

Herman, M., Balois, J. Y., Gonzalez, L., et al. (1986), Stratospheric aerosols observation from a balloon-borne polarimetric experiment, *Appl. Opt.* 25:3573–3584.

London, J., Bojkov, R. J., Oltmans, S., Kelley, J. I. (1976), Atlas of the global distribution of total ozone July 1957–June 1967, NCAR Technical Note No. 113 + STR.

Rouquet, M. C. (1987), Faisabilité de la calibration HRV-SPOT sur des cibles tests, Rapport Contrat CNES, Toulouse, France, 833 / CNES / 87 / 4891 / 00.

Santer, R. (1984), Caractérisation des aérosols à partir de la polarisation du rayonnement solaire diffusé. Application aux atmosphères de la Terre de Vénus et de Saturne, Thèse d'Etat, Lille.

Slater, P. N., Biggar, S. F., Holm R. D., et al. (1987), Reflectance and radiance-based methods for the in-flight absolute calibration of multispectral sensors, *Remote Sens. Environ.* 22:11–37.

Tanré, D., Deroo, C., Duhaut, P., et al. (1990), Description of a computer code to simulate the satellite signal in the solar spectrum: The 5S code, *Int. J. Remote Sens.* 11:659–668.

Vermote, E. (1990), Effects d'atmosphère en télédétection, Thèse Doctorat, Université des Sciences et Techniqes de Lille Flandres Artois (France).

Weinmann, J. A., Twilty, J. T., Browning, S. R., and Herman, B. M. (1975), Derivation of phase function from multiple scattered sunlight transmitted through a hazy atmosphere, *J. Atmos. Sci.* 32:577.